coatings

MDPI

Article

Plasma-Sprayed LSM Protective Coating on Metallic Interconnect of SOFC

Jia-Wei Chen [1], Kui-Yi Lin [1], Yung-Chin Yang [1,*] and Shu-Tuan Yeh [2]

[1] Institute of Materials Science and Engineering, National Taipei University of Technology, Taipei 106, Taiwan; cjw77213@yahoo.com.tw (J.-W.C.); tony821107@gmail.com (K.-Y.L.)

[2] Dental Department, Mackay Memorial Hospital, Taipei 106, Taiwan; fatchin@mail.mse.ncku.edu.tw

* Correspondence: ycyang@ntut.edu.tw; Tel.: +886-2-27712171; Fax: +886-2-27317185

Academic Editor: Morteza Eslamian

Received: 3 November 2017; Accepted: 9 December 2017; Published: 11 December 2017

Abstract: In this study, a $(La_{0.8}Sr_{0.2})_{0.98}MnO_3$ protective layer was prepared on the C276, Crofer22 APU, SUS304, and SUS430 alloys by the atmospheric plasma spraying technique (APS). The oxidation behavior and electrical property of these metal alloys have been investigated isothermally at 800 °C in air for up to 300 h. Results showed that the ferritic steels transform into $MnCr_2O_4$ spinels and a Cr_2O_3 layer during isothermal oxidation. The C276 alloy formed $NiCr_2O_4$ and $FeCr_2O_4$ layers; these are protective and act as an effective barrier against chromium migration into the outer oxide layer, and the alloy demonstrated good oxidation resistance and a reasonable match to the coefficient of thermal expansion of the substrate and a low-oxide scale area-specific resistance. The ASR effects on the formation of oxide scale have been investigated, and the ASR of coated samples was below 0.024 $\Omega \cdot cm^2$. It has good electrical conductivity for SOFC in long-term use.

Keywords: solid oxide fuel cell; metallic interconnect; plasma spray

1. Introduction

Solid oxide fuel cells (SOFCs) have recently attracted interest because of their high energy conversion efficiency, low pollution emission, effective waste-heat recovery, and relatively flexible fuel choice. The interconnection is an important component in the SOFCs, which provides electrical connection between contiguous cells as well as separation of the oxygen (cathode side) and fuel gases (anode side). Interconnected materials must possess the following characteristics: excellent electrical conductivity, corrosion resistance in oxidizing and reducing environment, and matched coefficient of thermal expansion (CTE) with other SOFC components. In recent years, metallic material systems have been investigated for interconnected applications including Fe-based [1–3], ZMG 232, Crofer22 APU; Cr-based [4], $Cr_5FeY_2O_3$; Ni-based alloys [5,6], Haynes 230, Haynes 242, Hastelloy S; Ni–Cr alloy systems; and so on. However, the Cr_2O_3 scale is known to release volatile oxides in the formation of CrO_3 or $CrO_2(OH)_2$, which takes place in the oxidizing environment of the SOFC cathode side [7]. The chromia-forming alloys have some inherent weakness, i.e., poisoning the cathode's electrochemical activity and drastically deteriorating SOFC performance under operating environments of SOFC due to Cr_2O_3 evaporation over long-term operation.

In order to reduce the rate of oxide scale growth and prevent chromium volatilization to the cathode side, coating a conductive ceramic/metal layer on alloys is an effective method. Many materials have been used to decrease oxide growth, increase oxide scale conductivity, improve adhesion between oxide scale and alloys, and inhibit Cr migration from substrate to the oxide surface. The materials adopted as coatings include reactive element oxides [8], perovskites [9], and spinels [10]. The coating techniques of the mentioned materials on stainless steels include sol–gel techniques [11], screen printing slurry coating [12,13], and magnetron sputtering [14]. The coating materials are the

perovskite materials with a chemical structure of ABO3, of which A and B are metallic cations: A is a large trivalent rare earth cation (e.g., La or Y) and B is usually a trivalent transition metal cation (e.g., Cr, Ni, Fe, Co, Cu or Mn). $La_{1-x}Sr_xMnO_3$ (LSM) is a widely used cathode material for SOFCs because of its excellent compatibility with other cell components and good performance at high temperatures.

LSM ceramic is also employed as a barrier on metallic interconnect by various coating processes. Lee et al. [12] reported that LSCF and LSM were coated on Crofer22 APU by screen printing and sintered over temperatures ranging from 1000 to 1100 °C in N_2. The ASR at 800 °C for the LSCF coated metal was less than the one coated with LSM. Hwang et al. [15] coated LSM on STS444 by aerosol deposition and thermal spray. They indicated that LSM coating by these two methods was not enough to prevent Cr evaporation from the interconnect to the cathode. Choi et al. [16] also used aerosol deposition to form a protective coating on the STS414 interconnect. The barrier materials employed were LSM–YSZ composite ceramics. The LSM–YSZ composite ceramics showed higher stability and electrical conductivity than the sole LSM layer at 800 °C, possibly due to the high microstructural stability of YSZ against grain growth at 800 °C. Palcut et al. [17] employed the plasma spray method to fabricate the LSM coating on Ceofer22 APU and four other kinds of metallic interconnect. The results show that the LSM coating acts as an oxygen transport barrier that can significantly reduce the corrosion rate. Base on the above research, a thermal sprayed LSM coating was shown to be denser and better at Cr prevention. In this study, we used the plasma spraying technique to deposit an LSM coating on the iron-based and nickel-based interconnect and investigate the phase transformation, area-specific resistance and microstructures for each metallic interconnect in detail.

2. Experiments

2.1. Materials

The investigated metallic materials were nickel-based alloys C276 and iron-based alloys: Crofer22 APU, SUS304, and SUS430 (YoungSing Metal Enterprise Co., Ltd., Tainan, Taiwan) were used for comparison. The chemical compositions of these alloys are listed in Table 1. The alloys were cut into rectangular samples of 10 × 10 × 1 mm^3 and each sample was ground to #1000 with SiC sand paper, cleaned in acetone, and dried.

Table 1. Compositions of alloys selected for interconnect (wt %).

Alloys	**Compositions**							
Fe-Based Alloys	**Fe**	**Cr**	**Mn**	**Ni**	**Si**	**Al**		**Total**
SUS 304	Bal.	19.16	1.41	8.38	0.64	0.18		100
SUS 430	Bal.	16.14	0.17	0.16	0.26	–		100
Crofer22 APU	Bal.	23.48	0.49	0.03	0.12	–		100
Ni-Based Alloys	**Ni**	**Cr**	**Mo**	**Fe**	**Mn**	**W**	**Co**	**Total**
C 276	Bal.	16.02	17.72	5.72	0.46	3.98	0.03	100

2.2. Plasma Spraying Process

Spray-dried lanthanum strontium manganese oxide (LSM) powder (Oerlikon Metco, Pfäffikon, Switzerland) with the composition $(La_{0.8}Sr_{0.2})_{0.98}MnO_3$ was used as the plasma spray feedstock. In experiments with high-power plasmas, the torch sprayed the feedstock onto substrates that were mounted on rotating machinery. For experiments, a robot moved the torch along a path to coat stationary substrates at a standoff distance. The substrates were cooled during spraying by air gun. The plasma spraying operating parameters were varied to determine the envelope of conditions in which it is possible to produce coatings of LSM. These parameters, including the plasma gas flow rate, the plasma gas composition, the arc current, and the nozzle size, are listed in Table 2.

Table 2. Parameters of plasma spraying for $(La_{0.8}Sr_{0.2})_{0.98}MnO_3$ (LSM) coating.

Spraying Parameters	LSM
Power (kW)	50
Torch current (A)	660
Primary gas (Ar) (L/min)	50
Secondary gas (H_2) (L/min)	14
Stand-off distance (cm)	10
Feedstock carrier gas (L/min)	3
Powder feed rate (rpm)	5
Surface speed, v_s (rpm)	150
Transverse speed, v_t (mm/s)	5
Spraying loop	3

2.3. Oxidation Test

Oxidation testing was performed on plasma-sprayed LSM-coated interconnects treated at 800 °C in air for 300 h; interconnects without coating were used as comparisons. The phase constituents of the precipitated oxide were identified by X-ray diffraction (XRD) (Bruker D2 Phaser, Bruker, Bremen, Germany). The surface morphologies and cross sections of the oxidized interlayer were observed by using scanning electron microscopy (SEM) (Hitachi S-4700, Hitachi, Ltd., Tokyo, Japan) with an energy dispersive spectroscopy (EDS) (Oxford Instruments, Oxfordshire, UK).

2.4. Area-Specific Resistance Measurement

The electrical resistance of oxidized specimens was measured by using a four-point method at 800 °C in air for 300 h. As shown in Figure 1, two of the oxidized surfaces were covered in Ag–Pd paste; moreover, Ag–Pd meshes attached with four Ag leads were placed on top of the paste for current collection. A constant current of 0.3 A was applied across two Ag leads using a power source; the corresponding voltage drop across the other two Ag leads was measured using a multimeter. A widely accepted parameter for scaling the electrical resistance of thermally grown oxide is area specific resistance (ASR). At each temperature, the resistance (R) was calculated according to Ohm's law, $R = (V/I)/2$. The ASR was equal to the R-value multiplied by the platinum electrode screen printing electrodes on the specimen area.

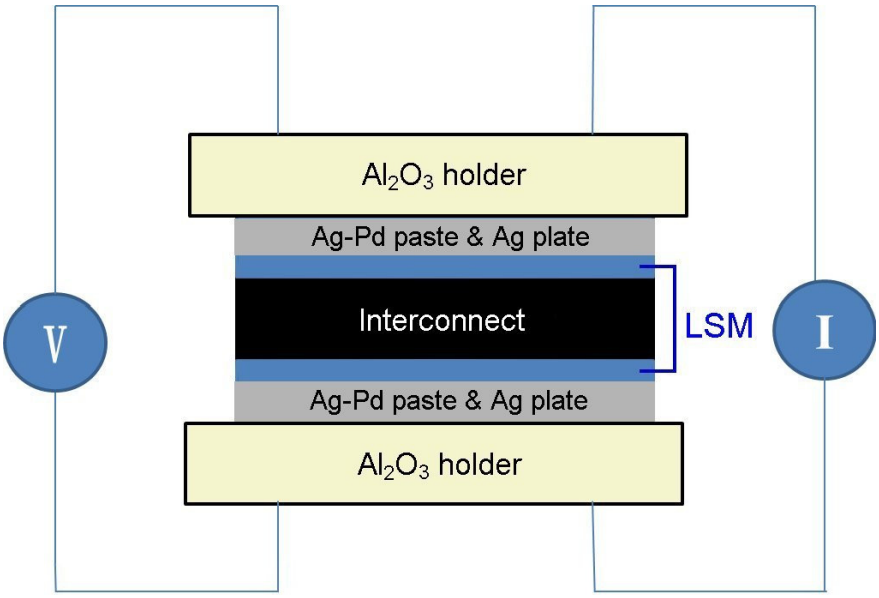

Figure 1. Schematic of the ASR measurement setup.

3. Results and Discussion

The cross-sectional microstructures of these four specimens are shown in Figure 2. As shown in Figure 2, oxide scale on the alloy without plasma-sprayed LSM displayed various types and thickness under the 800 °C heat treatment. It is obvious that the three iron-based metals, Crofer22 APU, SUS304 and SUS430, were oxidized with the formation of $MnCr_2O_4$ spinel and Cr_2O_3 phases (Supplementary Materials, Figure S1, full profile refinements are necessary to obtain more information about the XRD measurements). These metals oxidized at 800 °C include not only the Cr_2O_3 but also the $MnCr_2O_4$ spinel phase as the major phase; the manganese element in the substrate can be completely dissolved in Cr_2O_3, so often the Cr/Mn spinel structure appears in the outer oxide layer [18]. Crofer22 APU shows a thinner oxide scale than the other two, with a thickness of 2 to 5 μm (Figure 2). This is due to the high Cr content in the Crofer22 to form dense Cr_2O_3 and inhibit the growth of oxide scale. In addition to the Cr_2O_3, the $MnCr_2O_4$ also appeared in the oxide and formed on the outside of Cr_2O_3. For SUS304 and SUS430, the obvious $MnCr_2O_4$ spinel structure (part 2 in Figure 2c,d) could present on the outside of the Cr_2O_3 oxide (part 1 in Figures 2c and 3d). The total thickness of the oxide scale in SUS430 is 30 to 40 μm and 10 to 12 μm thick in SUS304. $MnCr_2O_4$ has a lower resistance than the other oxides and has the effect of preventing further oxidation of Cr_2O_3. This is because $MnCr_2O_4$ can prevent Cr from diffusing outwards and can inhibit Cr_2O_3 from contacting with oxygen. On the C276 alloy, in addition to the substrate phase of Ni–Cr–Mo, Cr_2O_3 $NiCr_2O_4$ and $NiFe_2O_4$ are the major phases in the oxide layer (Supplementary Materials, Figure S1). Fe_2O_3 and Cr_2O_3 dissolved to form a spinel structure of $FeCr_2O_4$ oxide. In C276 alloy $NiCr_2O_4$ spinel is also found, which is generated under high-temperature oxidation by the Cr_2O_3 and NiO reaction. The electrical conductivity of both $FeCr_2O_4$ and $NiCr_2O_4$ at higher temperatures are higher than that of Cr_2O_3 and precipitated on the outer layer, which helps reduce the oxidation and hinder the diffusion of chromium. The oxide scale of C276 in Figure 2a is very thin, around 1 to 3 μm.

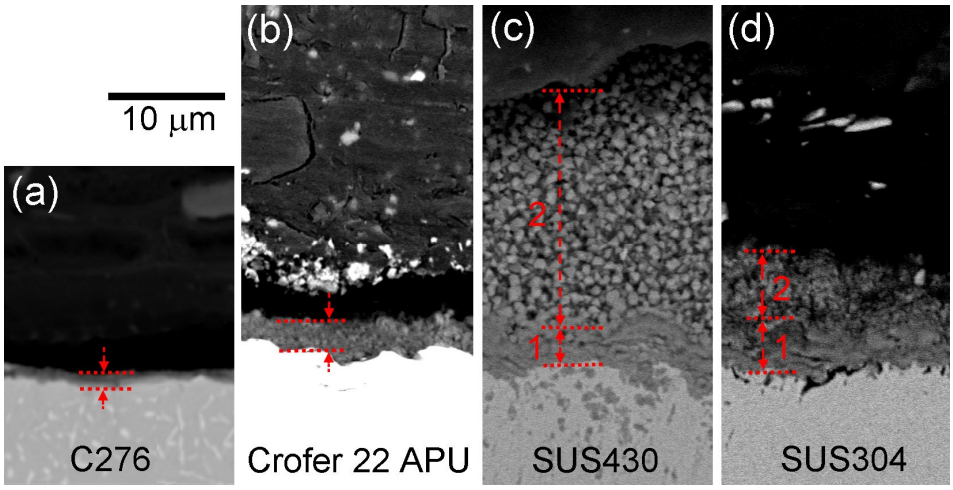

Figure 2. Cross-sectional views of the SUS430 and SUS304 alloy without LSM coating after oxidation at 800 °C for 300 h.

Cross-sectional views of the as-sprayed LSM coating on the metallic substrate are shown in Figure 3. The LSM was well deposited on the substrate, with 30–50 μm thickness. The CTE of four different substrates is similar to LSM and they mostly match. The thickness of the coating by APS is pretty uniform. There was no crack between the oxide layer and the substrate. Figure 4 showed cross-sectional views of the LSM/interconnect specimens after oxidation for 300 h in air at 800 °C. The structure of the LSM coating was stable and similar to the as-sprayed one. We can see the obvious oxidation formed in the interface between the coating and the substrate. There was a single phase of perovskite structure in the LSM coating (Supplementary Materials, Figure S2; full profile refinements

are necessary to obtain more information about the XRD measurements). No oxide was found in the LSM coating, which could indicate that the LSM coating can block Cr_2O_3 and $MnCr_2O_4$ from the metallic interconnect and result in the chromium elements finding it difficult to diffuse through the LSM coating to the LSM coating surface. The plasma-sprayed LSM layer can indeed effectively reduce the high-temperature oxidation of chromium oxide formed and decrease the outward diffusion of cathode poisoning.

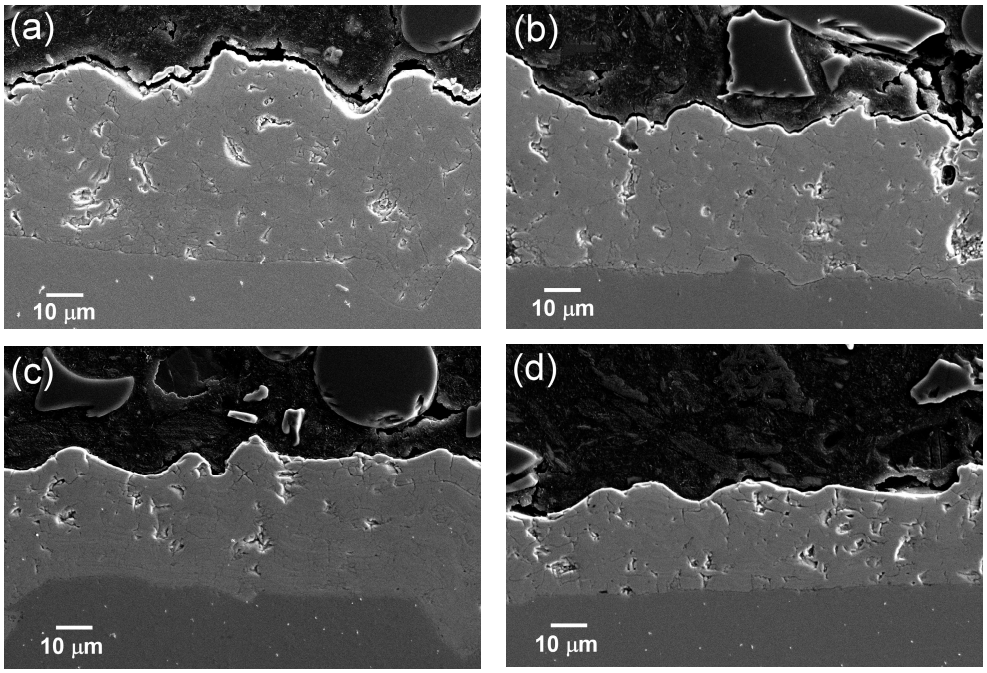

Figure 3. SEM cross-sectional views of the as-sprayed LSM coating on (**a**) C276; (**b**) Crofer22 APU; (**c**) SUS430; and (**d**) SUS304 interconnect.

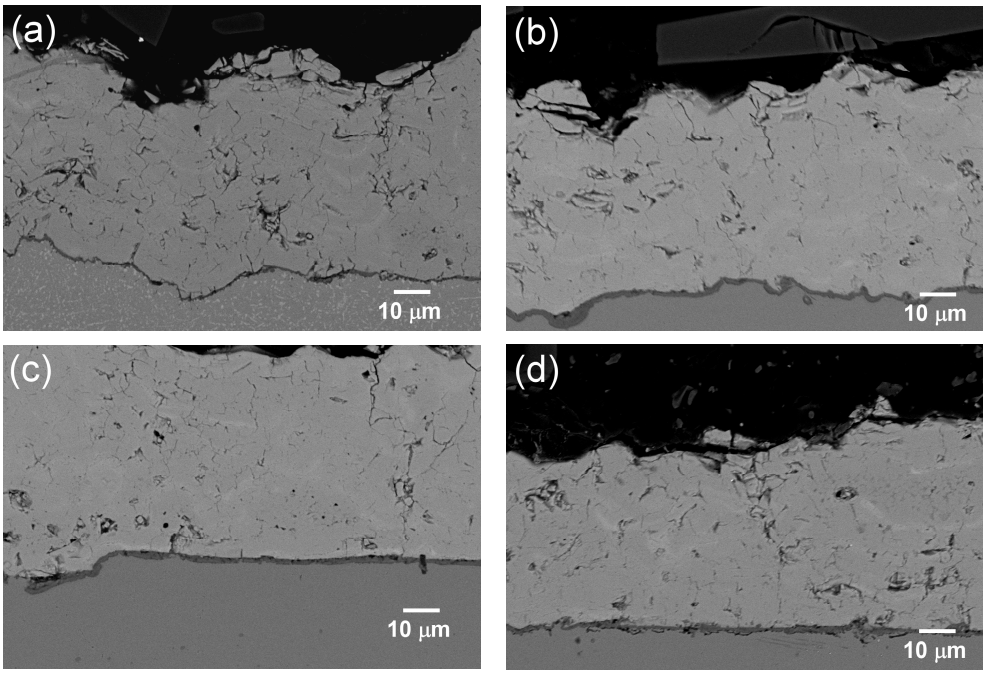

Figure 4. SEM cross-sectional views of the sprayed LSM coating on (**a**) C276; (**b**) Crofer22 APU; (**c**) SUS430; and (**d**) SUS304, after oxidation for 300 h in air at 800 °C.

The oxidation layer was evaluated. Figure 5 displayed the EDS line scan to analyze cross-sectional element distribution. Figure 5a shows that the oxide interlayer on C276 matches the substrate well and has an average thickness of 1–2 μm. From the element distribution in Figure 5a, the Cr_2O_3 layer has a thickness of 1 μm in the inner part of the oxide. Also, $MnCr_2O_4$ (ad maybe some $NiCr_2O_4$) existed on the outside of Cr_2O_3. The $MnCr_2O_4$ and $NiCr_2O_4$ spinel is desirable for better conducting performance. The $MnCr_2O_4$ spinel reduces the Cr diffusion into the LSM coating and provides higher conductivity at the SOFC working temperature.

Figure 5b,c reveal the oxide and element distribution of ferrite alloy Crofer 22 APU and SUS430. The oxide thickness formed (average thickness of 2–3 μm) in the coating was significantly less than that of the uncoated substrate in a similar situation, in which Cr_2O_3 and $MnCr_2O_4$ formed in the oxide scale at 800 °C. From the Cr distribution in Figure 5b,c, the Cr_2O_3 grew first in the substrate side and then Mn became enriched and diffused quickly outwards to Cr_2O_3, which caused the formation and rapid growth of a $MnCr_2O_4$ spinel in the LSM side. Mn/Cr/spinel could effectively inhibit the evaporation of Cr and reduce the growth rate of Cr_2O_3. Finally, chromia and spinel were major phases in its layer grown in air.

Figure 5d shows that there is less Mn in the oxide scale of SUS304 than in that of SUS430 and Crofer22 APU. The Cr_2O_3 was the main part of the oxide compared to the two kinds of substrate above. This would be confirmed by the ASR data due to the lower conductivity of Cr_2O_3 than $MnCr_2O_4$. In the substrate side, Fe diffused outwards to Cr_2O_3, which caused the formation of the $FeCr_2O_4$ spinel. On the other hand, a thin layer of $MnCr_2O_4$ was formed in the LSM side of the oxide. This dense layer was very important to limit the growth of the Cr_2O_3 and reduce its evaporation. LSM coating on the substrate blocks its contact with the oxygen in air; the oxidation behavior between the LSM coating and the substrate was due to a thermally grown oxide layer (TGO), causing a relatively dense and thin oxide layer on the surface.

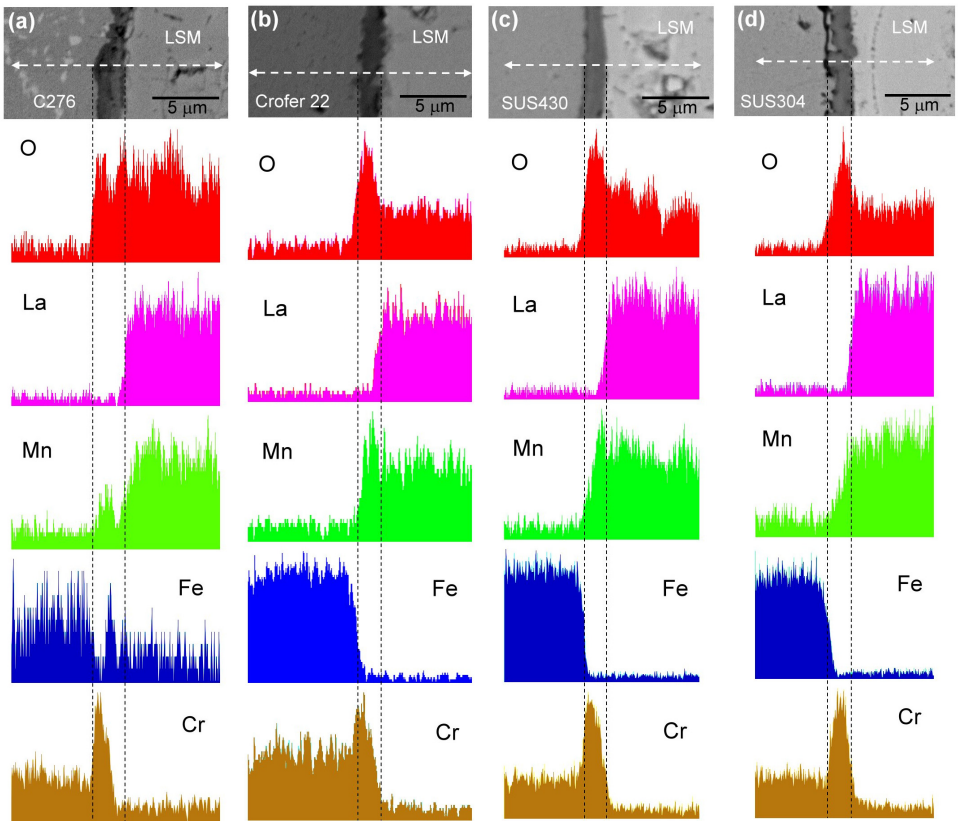

Figure 5. Element distribution analysis on the interface of the sprayed LSM coating on (**a**) C276; (**b**) Crofer22 APU; (**c**) SUS430; and (**d**) SUS304 alloy after oxidation for 300 h in air at 800 °C.

There is no oxide detected in the LSM protective coating due to the thickness (Supplementary Materials, Figure S2). Based on this, we can say that the Cr did not reach the surface of the LSM coating for 300 h in air at 800 °C. The LSM coating indeed prevents Cr from diffusing to the cathode. However, the LSM could react with Cr diffused from the substrate to form $LaCrO_3$, $(Cr, Mn)_3O_4$, or Cr_2O_3. The Cr evaporation is non-negligible. This was confirmed by the point scan in Figure 6. Even Cr could be inhibited in the oxide scale, but little of it could pass into the LSM coating. In the case of SUS304, Cr with 3.0 at % was detected in the position of LSM coating 3 μm from the oxide. No Cr was detected when the diffusion length was 3 μm from the oxide. The case was similar in SUS430: Cr with 0.49 at % was detected at the 2 μm position and no Cr was obtained in diffusion lengths of more than 6 μm. The diffusion length of Cr is dependent on the oxidation time and oxide thickness; the Cr will disperse further with a longer oxidation time.

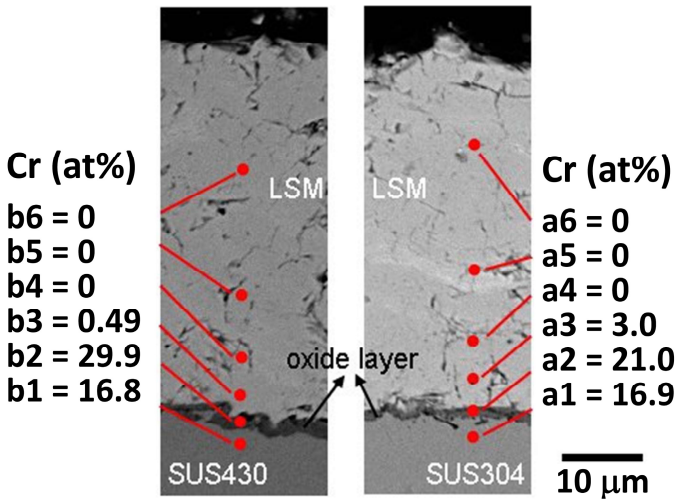

Figure 6. EDS point scan of chromium elements across the coating and substrate.

The ASR of four kinds of interconnect and plasma-sprayed LSM-coated alloys after oxidation for 300 h in air at 800 °C are shown in Figure 7. The ASRs for all LSM-coated alloys of interest in the present study are as follows: SUS 304 > SUS 430 > Crofer22 APU > C 276. The same rankings for the metal interconnects without LSM coating are also shown. Metal alloys without plasma-sprayed LSM coating displayed much higher resistance than the LSM protective interconnect. The higher resistance was contributed by the oxide thickness. Results from Figures 2 and 4: the oxide scale on the substrate without LSM coating is 5–10 times thicker than the LSM protective one. The decreased ASR of an LSM-coated interconnect indicates that the plasma-sprayed LSM coating indeed functions as a protective barrier. An iron-based alloy, SUS304, showed thinner oxide scale than SUS430 (Figure 2), but it displayed the highest resistance. This was due to the Cr diffusing quickly to form a thicker Cr_2O_3 layer than SUS430 (part 1 in Figure 2). The ASR of the SS304 was 0.024 $\Omega \cdot cm^2$, which was the worst conductivity. Crofer22 APU had a low impedance and its oxidation resistance properties were better than those of other iron-based alloys; the ASR of the Crofer22 APU was 0.01 $\Omega \cdot cm^2$, which proves the effectiveness of the LSM coating as a barrier to oxidation by inhibiting Cr diffusion and oxygen inside diffusion to thicken Cr_2O_3 and form $MnCr_2O_4$. For the nickel-based alloy C276, the ASR was significantly lower than the others; the ASR of the C276 was 0.0042 $\Omega \cdot cm^2$, which meets the requirements of interconnects for SOFCs. C276 was characterized by the formation of a $NiCr_2O_4$ spinel and a $NiFe_2O_4$ layer on top of the inner Cr_2O_3 layer, such that a low ASR is attributed to the higher electrical conductivity of both $NiCr_2O_4$ and $NiFe_2O_4$ than of Cr_2O_3 and $MnCr_2O_4$; these also indicated the potentially low Cr vaporization of the oxide scale of the alloy. Thus, it is interesting to investigate the Cr poisoning and deposition effects of the interconnect materials on cathodes. As this ASR test demonstrates, LSM is an excellent protective coating material for metallic interconnects of SOFCs.

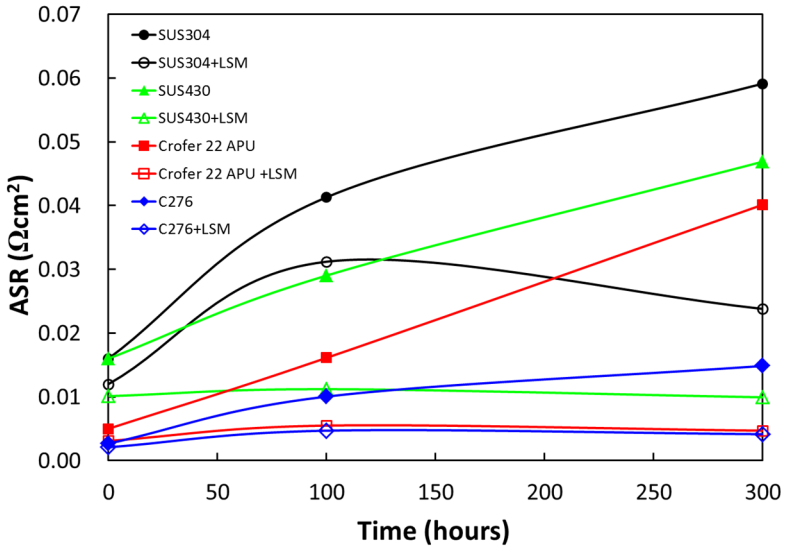

Figure 7. The ASR of plasma-sprayed LSM-coated alloys after oxidation for 300 h in air at 800 °C.

4. Conclusions

The effects of plasma-sprayed LSM coating were evaluated in air at 800 °C as a protective barrier to oxidation for the C276, Crofer22 APU, SUS430 and SS304 alloys as metallic interconnect materials, and the following conclusions can be made based on the obtained results.

- The plasma spraying method is a convenient method to generate a LSM coating on C276, Crofer22 APU, SUS430 and SUS304 alloys. An LSM coating has a thickness of 30–50 μm. The LSM layer is found to be quite dense, with few closed pores and without cracking. The XRD results indicated that the LSM protective layer could inhibit or delay Cr diffusing to the cathode.
- The oxide scale of the LSM-coated Crofer22 APU, SUS304 and SUS430 iron-based alloys after oxidation for 300 h in air at 800 °C consists of an inner layer of Fe/Mn-doped Cr_2O_3 and an outer layer of Fe-doped $MnCr_2O_4$. The growth of Cr_2O_3 and formation of $MnCr_2O_4$ potentially alleviate the Cr poisoning and deposition. The oxide scale of the LSM-coated C276 alloy after oxidation for 300 h in air at 800 °C consists of an inner layer of dense Cr_2O_3 and an outer layer of $NiCr_2O_4$ and few $NiFe_2O_4$. The formation of $NiCr_2O_4$ reduces Cr evaporation by separating the inner Cr_2O_3 layer from direct exposure to the environment.
- LSM-coated C276, Crofer22 APU, SUS430 and SUS304 alloys had lower resistances between 0.0042 and 0.024 $\Omega \cdot cm^2$ at 800 °C. The LSM layer is an excellent coating material for metallic interconnections, and has the potential to be used in SOFC applications.

Supplementary Materials: The following are available online at http://www.mdpi.com/2079-6412/7/12/226/s1, Figure S1: X-ray diffraction pattern of C276, Crofer22 APU, SUS430, and SUS304 alloys after oxidation at 800 °C for 300 h; Figure S2: X-ray diffraction pattern of the plasma sprayed LSM-coated C276, Crofer22 APU, SUS430 and SUS304 alloys after oxidation for 300 h in air at 800 °C.

Acknowledgments: The authors acknowledge financial support from the National Taipei University of Technology–Mackay Memorial Hospital Joint Research Program (NTUT-MMH-TT-99-10). We would also like to acknowledge the instrument and manpower support of the Metallurgy Division, Institute of Materials & Electro-Optics, Chung-Shan Institute of Science & Technology, Taiwan.

Author Contributions: Yung-Chin Yang conceived and designed the experiments; Jia-Wei Chen performed the experiments; Jia-Wei Chen and Kui-Yi Lin analyzed the data; Shu-Tuan Yeh contributed analysis tools; Jia-Wei Chen and Kui-Yi Lin wrote the paper.

Conflicts of Interest: The authors declare no conflict of interest.

References

1. Yang, Z.; Hardy, J.S.; Walker, M.S.; Xia, G.; Simner, S.P.; Stevenson, J.W. Structure and conductivity of thermally grown scales on ferritic Fe-Cr-Mn steel for SOFC interconnect applications. *J. Electrochem. Soc.* **2004**, *151*, A1825–A1831. [CrossRef]
2. Horita, T.; Xiong, Y.; Yamaji, K.; Sakai, N.; Yokokawa, H. Stability of Fe–Cr alloy interconnects under CH_4–H_2O atmosphere for SOFCs. *J. Power Sources* **2003**, *118*, 35–43. [CrossRef]
3. Zhu, W.Z.; Deevi, S.C. Development of interconnect materials for solid oxide fuel cells. *Mater. Sci. Eng. A* **2003**, *348*, 227–243. [CrossRef]
4. Konysheva, E.; Penkalla, H.; Wessel, E.; Mertens, J.; Seeling, U.; Singheiser, L.; Hilpert, K. Chromium poisoning of perovskite cathodes by the ODS alloy $Cr_5Fe_1Y_2O_3$ and the high chromium ferritic steel Crofer22APU. *J. Electrochem. Soc.* **2006**, *153*, A765–A773. [CrossRef]
5. England, D.M.; Virkar, A.V. Oxidation kinetics of some nickel-based superalloy foils and electronic resistance of the oxide scale formed in air. Part I. *J. Electrochem. Soc.* **1999**, *146*, 3196–3202. [CrossRef]
6. Yang, Z.; Xia, G.-G.; Stevenson, J.W. Evaluation of Ni-Cr-base alloys for SOFC interconnect applications. *J. Power Sources* **2006**, *160*, 1104–1110. [CrossRef]
7. Hilpert, K.; Das, D.; Miller, M.; Peck, D.H.; Weiß, R. Chromium vapor species over solid oxide fuel cell interconnect materials and their potential for degradation processes. *J. Electrochem. Soc.* **1996**, *143*, 3642–3647. [CrossRef]
8. Riffard, F.; Buscail, H.; Caudron, E.; Cueff, R.; Issartel, C.; Perrier, S. Effect of yttrium addition by sol-gel coating and ion implantation on the high temperature oxidation behaviour of the 304 steel. *Appl. Surf. Sci.* **2002**, *199*, 107–122. [CrossRef]
9. Choi, J.J.; Lee, J.H.; Park, D.S.; Hahn, B.D.; Yoon, W.H. Oxidation resistance coating of LSM and LSCF on SOFC metallic interconnects by the aerosol deposition process. *J. Am. Ceram. Soc.* **2007**, *90*, 1926–1929. [CrossRef]
10. Ringuedé, A.; Bronine, D.; Frade, J.R. Assessment of Ni/YSZ anodes prepared by combustion synthesis. *Solid State Ionics* **2002**, *146*, 219–224. [CrossRef]
11. Zhang, W.; Pu, J.; Chi, B.; Jian, L. $NiMn_2O_4$ spinel as an alternative coating material for metallic interconnects of intermediate temperature solid oxide fuel cells. *J. Power Sources* **2011**, *196*, 5591–5594. [CrossRef]
12. Lee, S.; Chu, C.L.; Tsai, M.J.; Lee, J. High temperature oxidation behavior of interconnect coated with LSCF and LSM for solid oxide fuel cell by screen printing. *Appl. Surf. Sci.* **2010**, *256*, 1817–1824. [CrossRef]
13. Yang, Z.; Xia, G.; Simner, S.P.; Stevenson, J.W. Thermal growth and performance of manganese cobaltite spinel protection layers on ferritic stainless steel SOFC interconnects. *J. Electrochem. Soc.* **2005**, *152*, A1896–A1901. [CrossRef]
14. Park, S.; Kumar, S.; Na, H.; Lee, C. Effects of sliver addition on properties and performance of plasma sprayed $La_{0.6}Sr_{0.4}Fe_{3-\delta}$. *J. Therm. Spray Technol.* **2008**, *17*, 708–714. [CrossRef]
15. Hwang, H.; Choi, G.M. The effects of LSM coating on 444 stainless steel as SOFC interconnect. *J. Electroceram.* **2009**, *22*, 67–72. [CrossRef]
16. Choi, J.J.; Ryu, J.; Hahn, B.D.; Yoon, W.H.; Lee, B.K.; Choi, J.H.; Park, D.S. Oxidation behavior of ferritic steel alloy coated with LSM–YSZ composite ceramics by aerosol deposition. *J. Alloys Compd.* **2010**, *492*, 488–495. [CrossRef]
17. Palcut, M.; Mikkelsen, L.; Neufeld, K.; Chen, M.; Knibbe, R.; Hendriksen, P.V. Improved oxidation resistance of ferritic steels with LSM coating for high temperature electrochemical applications. *Int. J. Hydrogen Energy* **2012**, *37*, 8087–8094. [CrossRef]
18. Ziomek, M.M.; Adler, T.; King, P. Materials Performance of Ferritic Steel in Combustion GASES for Heat Exchanger Applications in Solid Oxide Fuel Cell System. In Proceedings of the CORROSION 2008, New Orleans, LA, USA, 16–20 March 2008; NACE International Corrosion Conference Series; NACE-08460.